Isotropic and Anisotropic *g*-Factor Corrections in GaAs Quantum Dots

Leon C. Camenzind,[1,*] Simon Svab,[1,*] Peter Stano[2,3] Liuqi Yu[1,†] Jeramy D. Zimmerman,[4,‡]
Arthur C. Gossard,[4] Daniel Loss[1,2] and Dominik M. Zumbühl[1,¶]

[1]*Department of Physics, University of Basel, Basel 4056, Switzerland*
[2]*Center for Emergent Matter Science, RIKEN, Saitama 351-0198, Japan*
[3]*Institute of Physics, Slovak Academy of Sciences, 845 11 Bratislava, Slovakia*
[4]*Materials Department, University of California, Santa Barbara, California 93106, USA*

We experimentally determine isotropic and anisotropic *g*-factor corrections in lateral GaAs single-electron quantum dots. We extract the Zeeman splitting by measuring the tunnel rates into the individual spin states of an empty quantum dot for an in-plane magnetic field with various strengths and directions. We quantify the Zeeman energy and find a linear dependence on the magnetic field strength that allows us to extract the *g* factor. The measured *g* factor is understood in terms of spin-orbit interaction induced isotropic and anisotropic corrections to the GaAs bulk *g* factor. Experimental detection and identification of minute band-structure effects in the *g* factor is of significance for spin qubits in GaAs quantum dots.

Spins in semiconductor quantum dots are candidates for the realization of a scalable quantum bit (qubit) [1,2]. The energy of such a spin qubit is the Zeeman energy $\Delta = g\mu_B B$, where μ_B is the Bohr magneton, B is the magnetic field, and g is the g factor. In semiconductors, electric fields modify the confined-electron g factor and its generalization, the g tensor [3,4]. These corrections arise through the spin-orbit interaction (SOI) [5,6] imprinted in the material band structure. Understanding and exploiting such spin-orbit effects is a cornerstone of semiconducting spin qubits.

Indeed, while understanding the g factor gives insight into the fundamental physics of the confined spin, its control is important for qubit manipulation and coherence. The SOI-mediated [7–9] and micromagnet-induced [10,11] electric dipole spin resonance exemplify electrically based manipulations, while on-chip microwave antennas [12,13] provide magnetic drive. In multiqubit devices, local g-factor differences allow one to address qubits selectively and can also induce quantum logic gates [14,15]. On the other hand, being sensitive to the local electric field, the g factor and thus the qubit energy will fluctuate due to charge noise, resulting in decoherence [16,17]. This will be an issue, especially in group-IV semiconductor materials with little or no nuclear spins, e.g., silicon [3,13,18,19], Si/SiGe heterostructures [11], Ge/SiGe heterostructures [20], and Si/Ge nanowires [17].

In this Letter, we experimentally separate the isotropic and anisotropic g-factor corrections in two GaAs spin qubit devices with slightly different wafer properties. Thereby, we access small corrections to the g factor, previously beyond reach [21,22], and identify their band-structure origin. To do this, it is essential to rule out effects arising from

electron-electron interactions, which we achieve by measuring in the single-electron regime. Further, it is important to characterize the quantum dot confinement quantitatively by employing the spectroscopy methods developed in Ref. [23].

We compare the measurements to the theory of Ref. [6], which calculates the g-factor corrections of a single electron in a 2DEG quantum dot, arising within the so-called Ogg-McCombe Hamiltonian [24,25]. This Hamiltonian is derived within the $\mathbf{k} \cdot \mathbf{p}$ theory including higher-order, up to the fourth order in momentum, kinetic-energy terms in the band structure of GaAs. For typical quantum dot sizes and 2DEG widths, Ref. [6] finds that several terms have a notable effect on the g factor: while the isotropic correction is dominated by a time-reversal-antisymmetric SOI and the Rashba SOI, the anisotropy is due to the Dresselhaus SOI alone. With the only input being the 2DEG width, calibrated independently for our samples, the model predicts these two corrections with magnitudes of order 0.1 and 0.02, respectively. While much smaller than the bulk value (in magnitude 0.44), we can detect both of these corrections experimentally. Since the measured corrections are in reasonable agreement with the theory predictions without any fitting parameters, we believe that we have succeeded in confirming these predictions in our experiment.

The experiment was performed on two separate quantum dots, each in the single-electron regime, with adjacent quantum dot charge sensors [see Fig. 1(a)] on two different 2DEGs (see Sec. 1 [26] for details). The crystal axes were tracked from the wafer flats. The quantum dot is tunnel coupled only to the left reservoir. The sensor conductance reads the charge state [27,28] with a bandwidth of ~ 30 kHz. The device is on a piezo rotator (Attocube ANRv51), allowing magnetic fields up to 14 T in an
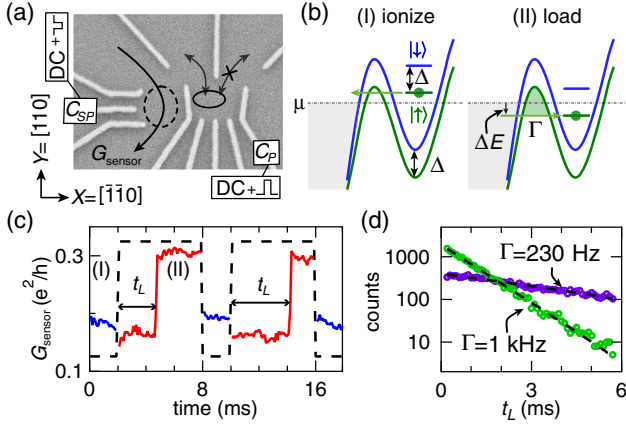
FIG. 1. (a) Electron micrograph of a cofabricated device with dot position (solid ellipse) and sensor dot (dashed ellipse). The sensor conductance G_{sensor} reads the real-time charge state of the dot. (b) A two-step pulse—(I) ionize and (II) load—is applied on the dot gate C_P to measure the tunneling rate Γ into the empty dot for detuning ΔE from the reservoir chemical potential μ. The sensor plunger C_{SP} is compensated to maintain readout sensitivity. A magnetic field splits the dot states $|\uparrow\rangle, |\downarrow\rangle$ as well as the conduction band (blue and green) by the Zeeman energy Δ. (c) Sensor conductance G_{sensor} for two cycles (dashed pulses). Low (high) G_{sensor} indicates an empty (occupied) dot, respectively. The ionization rate during (I) is faster than the sensor bandwidth. The electron loading times t_L, appearing as clear steps (red traces), are histogrammed to extract the tunnel rate Γ via exponential fit, shown in (d) for two examples, with typical error bars ± 10 Hz.

arbitrary in-plane direction. The misalignment is $< 2°$ and thus negligible [29]. Measurements are carried out at an electron temperature of 200 mK. To calculate the Zeeman energy Δ, it is necessary to convert changes of the voltages on plunger gate C_P to energy [see Fig. 1(b)]. For details of the calibration and the (negligible) dot shape dependence, see Secs. 1 and 2 in Ref. [26].

We obtain g by measuring the tunnel rate Γ into the spin states of an empty quantum dot, taking advantage of the increase in Γ when both spin states are energetically available. From these rates we extract Δ, and from the dependence of Δ on the magnetic field strength we fit g. We measure Γ by applying a two-step pulse to plunger gate C_P [see Fig. 1(a)], repeatedly ionizing and loading the quantum dot as shown by the energy diagrams in Fig. 1(b): to ionize, the energy level of the charged quantum dot is pulsed above the chemical potential μ of the reservoir such that an electron will tunnel out. We chose this ionization pulse such that the ionization efficiency is close to unity. To load, we pulse the empty quantum dot to an energy detuning ΔE below μ. At this energy, filled states are available in the reservoir and an electron can elastically tunnel through the barrier into the quantum dot. The time constant of this probabilistic tunnel process is given by Γ.

We obtain Γ by monitoring the charge sensor conductance G_{sensor} and extract the times of these loading events t_L

as shown in Fig 1(c): the tunneling of an electron leads to a change of the charge state from empty to loaded, which results in an observable switch to a higher G_{sensor}. We cycle through this pulse scheme between 2000 and 20 000 times and extract Γ by fitting an exponential function to a histogram of t_L [see Fig. 1(d)]. When changing the pulse amplitudes, we obtain Γ as a function of the detuning ΔE.

Three important comments about the experiment: First, to stay in the sweet spot of the sensor during the pulse sequence, we compensate the cross talk between the pulses applied to C_P and the sensor quantum dot by applying pulses of opposite polarity to the sensor plunger gate C_{SP} [see Fig. 1(a)] [30]. Second, we divide the total number of pulse cycles into segments in order to mitigate drift-related effects: In every segment, 100 pulses are applied at each selected detuning ΔE before an automated feedback loop is used to compensate for time-dependent drifts of the quantum dot levels by retrieving the position of $\Delta E = 0$ [31]. We exclude hysteresis effects by selecting the sequence of detunings ΔE to which we pulse randomly for each round. Third, due to the long timescale of the pulsing scheme [see Fig. 1(c)], we do not expect appreciable dynamic nuclear polarization.

In Fig. 2(a), we show data of $\Gamma(\Delta E)$ for increasing magnetic fields up to 12 T. Because of the orbital effects of the in-plane magnetic field [23], the tunnel barriers have to be readjusted for each field configuration in order to keep the tunnel rates at a few hundreds of Hz (see Sec. 4 in Ref. [26]). As a consequence, the magnitudes of $\Gamma(\Delta E)$ for the different traces are not comparable and were therefore normalized in Fig. 2(a). As the dot ground state is pulled below the reservoir and ΔE starts to increase from zero, electrons start to tunnel onto the dot, leading to the rising flank, as seen in Fig. 2(a) for $\Delta E \gtrsim 0$. The observed broadening is given by the reservoir temperature. As the dot level is pulled further below the reservoir, eventually the excited spin state becomes available, thus increasing the tunnel rate above the ground state rate, as indicated by the yellow arrow. The separation of the two steps is thus identified as the Zeeman splitting Δ and grows with the magnetic field, as seen on Fig. 2(a). The observed exponential suppression of $\Gamma \sim \exp(-\Delta E)$ is attributed to an effective increase of the tunnel barrier potential experienced by the electrons when the gate voltage is increased [32–35] (see Sec. 3 of Ref. [26]).

Next, we look at the magnetic field strength and direction dependence of the extracted Δ. We measure for magnetic fields applied in a range of directions between the crystallographic axes $[\bar{1}\,\bar{1}\,0]$ (X) and $[1\bar{1}0]$ (Y) [see Fig. 1(a)]. The measured Zeeman splittings Δ for device 1 are plotted in Fig. 2(b) (see Sec. 5 in Ref. [26] for device 2). We find a linear dependence for all directions, which indicates that the g factor is independent of the strength of the magnetic field. Accordingly, we use a linear fit (without offset) on
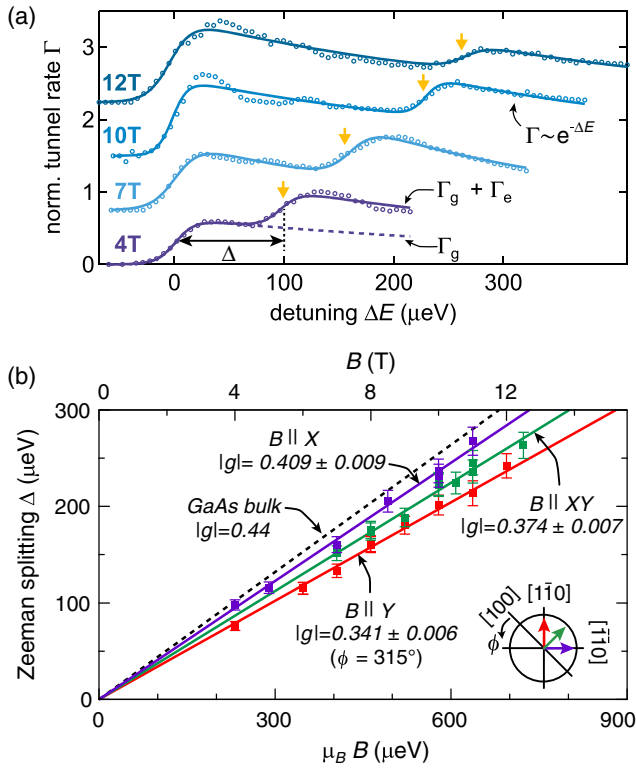
FIG. 2. (a) Examples of the normalized tunnel rate Γ into the empty quantum dot for different detunings ΔE and magnetic field strengths. Each trace exhibits two resonances, identified as the two spin states due to their behavior in the magnetic field (yellow arrows). The fits shown here are according to a phenomenological model described in Sec. 3 of Ref. [26]. In the trace taken at 4 T, the dashed line shows $\Gamma_g(\Delta E)$, the contribution of the spin ground state to the total tunnel rate, and Δ indicates the Zeeman splitting. (b) Zeeman splittings Δ in device 1, measured for different magnetic field strengths B and directions as indicated by the labels. The error bars reflect the statistical uncertainty from the fits. The slope is the absolute value of the g factor $|g| = \Delta/(\mu_B|B|)$ and differs from the GaAs bulk g factor due to spin-orbit interaction induced corrections. A distinct g-factor anisotropy is observed in the data. The inset shows the direction of the applied magnetic fields with respect to the crystal axes.

these datasets to obtain $|g|$, the absolute value of g. The statistical uncertainty obtained from the fits is in the range of a 1% relative error. Also, it was not possible to obtain a reliable Δ at some specific B values and directions due to vanishing excited spin tunneling [31,36] and/or due to measurement artifacts such as reservoir resonances.

Strikingly, the data show that g depends on the magnetic-field direction. For device 1, the g factor is maximal for a field along X with $|g| \approx 0.406$, and minimal along Y, where $|g| \approx 0.344$. This difference is well above the statistical error bar and similar in device 2 (see Sec. 5 in Ref. [26]). This is in good qualitative agreement with the theory in Ref. [6]. In that model, there are numerous terms giving corrections to the bulk g factor. These can be separated into an isotropic and an anisotropic part, such that

$$g = g_{\text{bulk}} + \delta g_i + \delta g_a \cos(2\phi + \pi/2), \qquad (1)$$

where $g_{\text{bulk}} = -0.44$ is the GaAs bulk g factor and ϕ defines the in-plane angle with respect to the main crystal axis [100] [see inset in Fig. 2(b)]. Here, terms with higher-order angle dependence are small and are neglected. We extract δg_i and δg_a experimentally, and the quantification of these two parameters for our quantum dot is the main result of this Letter. For most of the relevant terms, the magnitudes of the g-factor corrections depend primarily on λ_z, the effective width of the electron wave function along the growth direction [6]. Here, λ_z is given by the triangular confinement potential formed by the GaAs/AlGaAs heterostructure. We fit it from excited orbital state data and find $\lambda_z \approx 6.5$ nm similar for both devices [23,37] (see Sec. 2 in Ref. [26]).

We compare the experimental finding to the theoretical prediction for the magnetic field along Y and the specific quantum dot confinement of device 1. We obtain δg, the g-factor correction from g_{bulk}, from the measurement at each individual magnetic field by calculating $\delta g = |g_{\text{bulk}}| - |\Delta/(\mu_B B)|$. As seen in Fig. 3(a), the data of the two devices are in agreement with each other within the error bars (apart from one outlier) and show a slight trend to decrease at large fields. Also, with most data points slightly below the green theory curve, it seems fairly clear that the theory overall predicts a somewhat larger correction than measured in experiment. While only one specific direction is plotted here, we find this discrepancy generally for the isotropic correction. The model predicts an average $|\bar{g}| = |g_{\text{bulk}} + \delta g_i| \approx 0.33$ for an electron confined in such a quantum dot. The data presented in Fig. 2(b) suggest an isotropic correction to $|\bar{g}| \approx 0.373$ for device 1 and $|\bar{g}| \approx 0.396$ for device 2. Thus, the theory calculates a stronger isotropic correction than seen in the experiment—to be discussed later.

The theory predicts several terms contributing to the isotropic correction δg_i, as shown on Fig. 3(a). The largest two are δg_R, a correction due to the intrinsic Rashba SOI appearing with the structural inversion asymmetry, and δg_{43}, a correction due to the magnetic-field-induced SOI term H_{43} [6,25]. The essential difference is the behavior under the time-reversal symmetry: the two SOI terms are symmetric and antisymmetric, respectively. The next strongest isotropic term is the penetration correction δg_p, which arises from the overlap of the wave function with the AlGaAs bulk where $g_{\text{AlGaAs}} = +0.4$ [38]. This term is negligible in our case but becomes substantial for smaller 2DEG widths ($\lambda_z \lesssim 4$ nm).

The anisotropic correction to the g factor originates from the Dresselhaus SOI, which is a consequence of bulk inversion asymmetry in the zinc blende crystal structure of GaAs. As seen in Fig. 2(b), the largest correction to g_{bulk} is observed along Y. This finding indicates that the Dresselhaus constant γ_c is negative since a positive γ_c would result in the largest deviation from g_{bulk} in the X
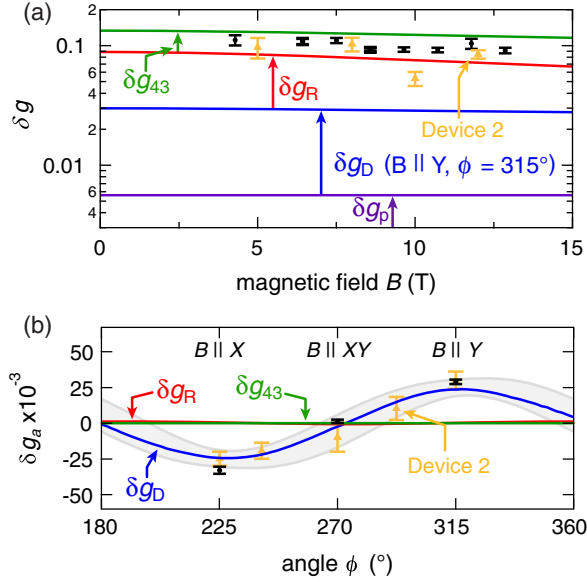
FIG. 3. (a) Cumulative g-factor corrections δg to g_{bulk} as labeled. The isotropic terms are due to penetration into the AlGaAs, δg_p, due to the H_{43} term, δg_{43}, and the Rashba correction, δg_R. The magnetic field dependence of δg_R arises from an interference of the Rashba term and orbital effects. The Dresselhaus correction, δg_D, is anisotropic and given for a field along Y ($\phi = 315°$), the same direction for which the data are shown (black device 1, yellow device 2). Here, the g-factor corrections at the respective magnetic fields are directly obtained from the individual measured Zeeman splitting. The green curve shows the total theoretical g-factor correction for this field direction. (b) The anisotropic corrections to the g factor are dominated by δg_D, while δg_R and δg_{43} give insignificant anisotropic corrections. The gray band indicates the 1σ confidence interval of a sine fit to the data of device 2 with a fixed period of 180°. Note that the blue trace (δg_D) is a plot of the model, not a fit.

direction [6]. Concerning the sign of γ_c, which remains somewhat controversial [39,40], our results thus agree with Ref. [39]. We get $\delta g_a = 0.030 \pm 0.002$ for device 1 and 0.025 ± 0.003 for device 2, which is close to the predicted $\delta g_a = 0.024$. Further, for the relative correction to the g factor, we find $\delta g_a/|\bar{g}| \approx 8.1 \pm 0.5\%$ for device 1 and $\approx 6.3 \pm 0.8\%$ for device 2, which is in good agreement with the model where this ratio is $\approx 7\%$.

We now discuss the possible origins of the discrepancy between theory and experiment in the isotropic correction. The first suspect is the lever arm used to convert the gate voltage on C_P to detuning ΔE: the accuracy of the mixing chamber temperature used to determine the lever arm [23,41] is about 5–10% at worst. However, because—as confirmed by experiment—the lever arm is independent of both the strength and direction of the field, an error in the lever arm would rescale all measured g-factor values by the same factor. This is, however, not sufficient to reconcile the theory with the data from both devices. In addition, the precision of the measurement originating from the

statistical uncertainty is much better, around 1%, allowing us to compare, for example, g factors along different directions with high resolution.

Another source of deviations could be that the constants used for the $\mathbf{k} \cdot \mathbf{p}$ calculations in the model were off: these parameters are notoriously difficult to quantify in theory and experiments [40]. From the data measured here, it is also not possible to conclude which term leads to the overestimation of δg_i when compared to the experiment.

Simplifications in the model of the heterointerface can also lead to a deviation from the observed g factor: the model assumes an infinite linear slope of the triangular confinement potential and a steplike increase of the aluminum concentration at the AlGaAs/GaAs interface. In reality, the profile is different in both aspects: the linear slope levels off away from the interface and there is a finite transition region from AlGaAs to GaAs. Perhaps most importantly here, the details of the interface on the atomic level can effectively induce additional spin-orbit interactions [3,4,42,43].

Finally, we mention the possibility that one needs to go beyond $\mathbf{k} \cdot \mathbf{p}$ theory. For example, Ref. [44] reports on self-assembled InGaAs/GaAs quantum dots that are so small and strongly strained that the structure inhomogeneities impose strong deviations from properties based on bulk crystal models. However, this scenario is rather improbable for our large and weakly strained (lattice matched) gated GaAs/AlGaAs dots. On the other hand, strain effects could be a source of the discrepancy in principle, as Ref. [6] does not include strain. While leaving the full account for a separate publication, our preliminary analysis shows that strain of order $10^{-4} - 10^{-3}$ [45] probably does not suffice to explain the discrepancies. However, since the amount of strain in our devices is unknown, we do not make a definite conclusion about the source of discrepancy.

In summary, we find a clear g-factor anisotropy and isotropic correction to the bulk g factor in two quantum dots made on different GaAs/AlGaAs heterostructures. We compare our findings to the theory [6]: while the measured isotropic corrections are weaker than predicted, our data for the anisotropic corrections are in good agreement. The dominant isotropic corrections arise from the Rashba SOI and a magnetic-field-induced term δg_{43}, and the anisotropic correction originates from the Dresselhaus SOI only. In silicon spin qubits, the anisotropy gives a change of the g factor of the order of 1%, dominated by surface roughness [3,4]. In contrast, here, the measured anisotropy is larger, around 7%, due to the Dresselhaus SOI of the GaAs crystal.

Our findings substantiate the relevant g-factor corrections in GaAs spin qubits. Here, the dominant terms could help to better understand the decoherence from coupling to charge noise and might be exploited for all electrical spin manipulation. Furthermore, we probe the band-structure parameters in the absence of electron-electron interaction

effects in the singly occupied dot, which are otherwise often problematic. From the dependence of the g-factor corrections on the width and symmetry of the heterostructure, the $\mathbf{k} \cdot \mathbf{p}$ parameters could be obtained with a new level of confidence [6].

The data supporting this study are available in a Zenodo repository [46].

---

[*]These authors contributed equally to this work.
[†]Present address: Laboratory for Physical Sciences, 8050 Greenmead Drive, College Park, Maryland 20740, USA.
[‡]Present address: Physics Department, Colorado School of Mines, Golden, Colorado 80401, USA.
[¶]Corresponding author.
dominik.zumbuhl@unibas.ch

[1] D. Loss and D. P. DiVincenzo, Phys. Rev. A **57,** 120 (1998).
[2] C. Kloeffel and D. Loss, Annu. Rev. Condens. Matter Phys. **4,** 51 (2013).
[3] T. Tanttu, B. Hensen, K. W. Chan, C. H. Yang, W. W. Huang, M. Fogarty, F. Hudson, K. Itoh, D. Culcer, A. Laucht, A. Morello, and A. Dzurak, Phys. Rev. X **9,** 021028 (2019).
[4] R. Ferdous, K. W. Chan, M. Veldhorst, J. C. Hwang, C. H. Yang, H. Sahasrabudhe, G. Klimeck, A. Morello, A. S. Dzurak, and R. Rahman, Phys. Rev. B **97,** 241401(R) (2018).
[5] R. Winkler, *Spin-Orbit Coupling Effects in Two-Dimensional Electron and Hole Systems,* Springer Tracts in Modern Physics Vol. 191 (Springer, New York, 2003), https://doi.org/10.1007/b13586.
[6] P. Stano, C.-H. Hsu, M. Serina, L. C. Camenzind, D. M. Zumbühl, and D. Loss, Phys. Rev. B **98,** 195314 (2018).
[7] V. N. Golovach, M. Borhani, and D. Loss, Phys. Rev. B **74,** 165319 (2006).
[8] K. C. Nowack, F. H. L. Koppens, Y. V. Nazarov, and L. M. K. Vandersypen, Science **318,** 1430 (2007).
[9] A. Crippa, R. Maurand, L. Bourdet, D. Kotekar-Patil, A. Amisse, X. Jehl, M. Sanquer, R. Laviéville, H. Bohuslavskyi, L. Hutin, S. Barraud, M. Vinet, Y.-M. Niquet, and S. D. Franceschi, Phys. Rev. Lett. **120** (2018).
[10] M. Pioro-Ladrière, T. Obata, Y. Tokura, Y.-S. Shin, T. Kubo, K. Yoshida, T. Taniyama, and S. Tarucha, Nat. Phys. **4,** 776 (2008).
[11] J. Yoneda, K. Takeda, T. Otsuka, T. Nakajima, M. R. Delbecq, G. Allison, T. Honda, T. Kodera, S. Oda, Y. Hoshi, N. Usami, K. M. Itoh, and S. Tarucha, Nat. Nanotechnol. **13,** 102 (2018).
[12] F. H. L. Koppens, C. Buizert, K. J. Tielrooij, I. T. Vink, K. C. Nowack, T. Meunier, L. P. Kouwenhoven, and L. M. K. Vandersypen, Nature (London) **442,** 766 (2006).
[13] M. Veldhorst, J. C. C. Hwang, C. H. Yang, A. W. Leenstra, B. de Ronde, J. P. Dehollain, J. T. Muhonen, F. E. Hudson, K. M. Itoh, A. Morello, and A. S. Dzurak, Nat. Nanotechnol. **9,** 981 (2014).
[14] M. Veldhorst, C. H. Yang, J. C. C. Hwang, W. Huang, J. P. Dehollain, J. T. Muhonen, S. Simmons, A. Laucht, F. E. Hudson, K. M. Itoh, A. Morello, and A. S. Dzurak, Nature (London) **526,** 410 (2015).
[15] C. Jones, M. A. Fogarty, A. Morello, M. F. Gyure, A. S. Dzurak, and T. D. Ladd, Phys. Rev. X **8,** 021058 (2018).
[16] T. Nakajima, A. Noiri, K. Kawasaki, J. Yoneda, P. Stano, S. Amaha, T. Otsuka, K. Takeda, M. R. Delbecq, G. Allison, A. Ludwig, A. D. Wieck, D. Loss, and S. Tarucha, Phys. Rev. X **10,** 011060 (2020).
[17] F. N. M. Froning, L. C. Camenzind, O. A. H. van der Molen, A. Li, E. P. A. M. Bakkers, D. M. Zumbühl, and F. R. Braakman, Nat. Nanotechnol. **16,** 308 (2021).
[18] R. Maurand, X. Jehl, D. Kotekar-Patil, A. Corna, H. Bohuslavskyi, R. Laviéville, L. Hutin, S. Barraud, M. Vinet, M. Sanquer, and S. De Franceschi, Nat. Commun. **7,** 13575 (2016).
[19] L. C. Camenzind, S. Geyer, A. Fuhrer, R. J. Warburton, D. M. Zumbühl, and A. V. Kuhlmann, arXiv:2103.07369.
[20] N. W. Hendrickx, D. P. Franke, A. Sammak, G. Scappucci, and M. Veldhorst, Nature (London) **577,** 487 (2020).
[21] V. P. Michal, T. Fujita, T. A. Baart, J. Danon, C. Reichl, W. Wegscheider, L. M. K. Vandersypen, and Y. V. Nazarov, Phys. Rev. B **97,** 035301 (2018).
[22] D. M. Zumbühl, C. M. Marcus, M. P. Hanson, and A. C. Gossard, Phys. Rev. Lett. **93,** 256801 (2004).
[23] L. C. Camenzind, L. Yu, P. Stano, J. D. Zimmerman, A. C. Gossard, D. Loss, and D. M. Zumbühl, Phys. Rev. Lett. **122,** 207701 (2019).
[24] N. R. Ogg, Proc. Phys. Soc. **89,** 431 (1966).
[25] M. Braun and U. Rössler, J. Phys. C **18,** 3365 (1985).
[26] See Supplemental Material at http://link.aps.org/supplemental/10.1103/PhysRevLett.127.057701 for more details on the difference of the two devices, additional information on the tunnel rates into the spin states, and supporting data for device 2.
[27] M. Field, C. G. Smith, M. Pepper, D. A. Ritchie, J. E. F. Frost, G. A. C. Jones, and D. G. Hasko, Phys. Rev. Lett. **70,** 1311 (1993).
[28] C. Barthel, M. Kjærgaard, J. Medford, M. Stopa, C. M. Marcus, M. P. Hanson, and A. C. Gossard, Phys. Rev. B **81,** 161308(R) (2010).
[29] L. C. Camenzind, L. Yu, P. Stano, J. D. Zimmerman, A. C. Gossard, D. Loss, and D. M. Zumbühl, Nat. Commun. **9,** 3454 (2018).
[30] D. E. F. Biesinger, C. P. Scheller, B. Braunecker, J. Zimmerman, A. C. Gossard, and D. M. Zumbühl, Phys. Rev. Lett. **115,** 106804 (2015).
[31] S. Amasha, K. MacLean, I. P. Radu, D. M. Zumbühl, M. A. Kastner, M. P. Hanson, and A. C. Gossard, Phys. Rev. B **78,** 041306(R) (2008).

[32] K. MacLean, S. Amasha, I. P. Radu, D. M. Zumbühl, M. A. Kastner, M. P. Hanson, and A. C. Gossard, Phys. Rev. Lett. **98**, 036802 (2007).

[33] S. Amasha, K. MacLean, I. P. Radu, D. M. Zumbühl, M. A. Kastner, M. P. Hanson, and A. C. Gossard, Phys. Rev. Lett. **100**, 046803 (2008).

[34] P. Stano and P. Jacquod, Phys. Rev. B **82**, 125309 (2010).

[35] C. B. Simmons, J. R. Prance, B. J. Van Bael, T. S. Koh, Z. Shi, D. E. Savage, M. G. Lagally, R. Joynt, M. Friesen, S. N. Coppersmith, and M. A. Eriksson, Phys. Rev. Lett. **106**, 156804 (2011).

[36] M. Yamagishi, N. Watase, M. Hashisaka, K. Muraki, and T. Fujisawa, Phys. Rev. B **90**, 035306 (2014).

[37] P. Stano, C.-H. Hsu, L. C. Camenzind, L. Yu, D. Zumbühl, and D. Loss, Phys. Rev. B **99**, 085308 (2019).

[38] R. Hanson, B. Witkamp, L. M. K. Vandersypen, L. H. W. van Beveren, J. M. Elzerman, and L. P. Kouwenhoven, Phys. Rev. Lett. **91**, 196802 (2003).

[39] M. Studer, M. P. Walser, S. Baer, H. Rusterholz, S. Schn, D. Schuh, W. Wegscheider, K. Ensslin, and G. Salis, Phys. Rev. B **82**, 235320 (2010).

[40] Z. A. Devizorova, A. V. Shchepetilnikov, Y. A. Nefyodov, V. A. Volkov, and I. V. Kukushkin, JETP Lett. **100**, 102 (2014).

[41] D. Maradan, L. Casparis, T.-M. Liu, D. E. F. Biesinger, C. P. Scheller, D. M. Zumbühl, J. D. Zimmerman, and A. C. Gossard, J. Low Temp. Phys. **175**, 784 (2014).

[42] U. Rössler and J. Kainz, Solid State Commun. **121**, 313 (2002).

[43] L. E. Golub and E. L. Ivchenko, Phys. Rev. B **69**, 115333 (2004).

[44] G. Bester and A. Zunger, Phys. Rev. B **71**, 045318 (2005).

[45] M. H. Fauzi, M. F. Sahdan, M. Takahashi, A. Basak, K. Sato, K. Nagase, B. Muralidharan, and Y. Hirayama, Phys. Rev. B **100**, 241301(R) (2019).

[46] L. C. Camenzind, S. Svab, P. Stano, L. Yu, J. D. Zimmerman, A. C. Gossard, D. Loss, and D. M. Zumbühl, Supporting data for "Isotropic and Anisotropic g-factor Corrections in GaAs Quantum Dots", Zenodo, https://doi.org/10.5281/zenodo.3819014 (2020).